Methyl-branched lipids promote the membrane adsorption of α-synuclein by enhancing shallow lipid-packing defects

Matthias Garten,[abc] Coline Prévost,[abc] Clotilde Cadart,[abc] Romain Gautier,[d] Luc Bousset,[e] Ronald Melki,[e] Patricia Bassereau†[abc] and Stefano Vanni†*[d]

Alpha-synuclein (AS) is a synaptic protein that is directly involved in Parkinson's disease due to its tendency to form protein aggregates. Since AS aggregation can be dependent on the interactions between the protein and the cell plasma membrane, elucidating the membrane binding properties of AS is of crucial importance to establish the molecular basis of AS aggregation into toxic fibrils. Using a combination of *in vitro* reconstitution experiments based on Giant Unilamellar Vesicles (GUVs), confocal microscopy and all-atom molecular dynamics simulations, we have investigated the membrane binding properties of AS, with a focus on the relative contribution of hydrophobic *versus* electrostatic interactions. In contrast with previous observations, we did not observe any binding of AS to membranes containing the ganglioside GM1, even at relatively high GM1 content. AS, on the other hand, showed a stronger affinity for neutral flat membranes consisting of methyl-branched lipids. To rationalize these results, we used all-atom molecular dynamics simulations to investigate the influence of methyl-branched lipids on interfacial membrane properties. We found that methyl-branched lipids promote the membrane adsorption of AS by creating shallow lipid-packing defects to a larger extent than polyunsaturated and monounsaturated lipids. Our findings suggest that methyl-branched lipids may constitute a remarkably adhesive substrate for peripheral proteins that adsorb on membranes *via* hydrophobic insertions.

Introduction

Alpha-synuclein (AS) is a 140 a.a. protein that is particularly abundant in the central nervous system. Even though its physiological role is not yet perfectly understood, AS has been proposed to function in the maintenance of a supply of synaptic vesicles in presynaptic terminals.[1]

In addition, AS is directly involved in Parkinson's disease (For a comprehensive review, see for instance ref. 2). Like many other neurodegenerative diseases, the hallmark of Parkinson's disease (PD) are protein aggregates named "Lewy bodies"[3] whose main constituent is fibrillar AS. Since protein aggregation can be dependent on the interactions between the protein and the cell plasma membrane,[4] many efforts have been devoted to the understanding of the interactions between AS and model membranes.[5]

The N-terminal region of AS is essential for its interaction with membranes. Upon membrane binding, this region adopts a helical structure with a marked amphipathic character.[6,7] In contrast with other amphipathic helices (AHs), AS has a poorly developed hydrophobic face, mostly containing valine and alanine residues, and a large polar face that contains several charged residues. These structural features likely explain its marked sensitivity to both negatively charged lipids and membrane curvature.[5]

In addition, AS can strongly remodel membranes, promoting membrane thinning[8] and inducing membrane curvature by converting large vesicles into highly curved membrane tubules,[9] eventually leading to their fragmentation.[10] In some conditions, AS can permeabilize membranes by forming stable, pore-like oligomers (reviewed in ref. 2 and 11). In supported lipid bilayers, it has been proposed that AS disrupts the membrane by the extraction of lipids from the bilayer that cluster around AS aggregates.[12]

So far, the presence of negatively charged lipids has been shown to be necessary for AS binding.[7,11,13–15] It was also proposed that AS can specifically interact with gangliosides,[16] in particular with GM1,[17,18] which is highly enriched in synaptic regions of neurons.[19,20] Since gangliosides are mainly found in the extracellular leaflet of the plasma membrane, this observation could

[a] *Institut Curie, Centre de Recherche, Paris, France*
[b] *CNRS, laboratoire PhysicoChimie Curie, UMR 168, Paris, France*
[c] *Université Pierre et Marie Curie, Paris, France*
[d] *Institut de Pharmacologie Moléculaire et Cellulaire, Université de Nice Sophia-Antipolis and Centre National de la Recherche Scientifique, UMR 7275, 06560 Valbonne, France. E-mail: vanni@ipmc.cnrs.fr*
[e] *CNRS, Paris Saclay Institute of Neuroscience, Gif-sur-Yvette, France*
† These authors contributed equally to the manuscript.

partially explain how AS fibrils spreads between neurons,[21] thus contributing to PD progression. However, experiments were performed at ganglioside densities much higher than endogenous cellular levels,[16,18] and the exact role of GM1 in AS binding at the plasma membrane remains unclear.

In addition, it has been proposed that the presence of lipid-packing defects at the water–membrane interface may facilitate AS membrane binding,[22–24] by favoring the insertion of its hydrophobic face.[25] Recently, new *in silico* analyses based on molecular dynamics (MD) simulations have allowed the quantification of such lipid-packing defects in model membranes.[26–28] Moreover, a combination of coarse-grain MD simulations with liposome binding assays indicated that AS appears particularly sensitive to the presence of ''shallow'' lipid-packing defects that are found at the membrane–water interface and that do not extend deeply within the hydrophobic membrane core.[29] These defects can be promoted by either membrane deformations or by the presence of polyunsaturated lipids, thanks to the unique flexibility of the polyunsaturated acyl chain.[29]

So far, polyunsaturated lipids are the only lipid species that has been shown to specifically enhance this type of membrane defects. We hypothesized that shallow lipid-packing defects could also be promoted by lipids with bulky chains and a normal-sized head group (such as phosphocholine). This is the case of diphytanoyl phosphocholine (DPhPC), a lipid with fully saturated, methyl-branched chains that is found essentially in bacteria and extremophilic archaea.[30,31] Due to its high stability and resistance to electroporation,[32] DPhPC has been extensively employed in electrophysiological measurements[33,34] and for the study of the interactions between lipid bilayers and proteins, in particular channel-forming peptides.[35–37] Nonetheless, the potential interactions of AS, and of AHs in general, with this lipid type have not been investigated so far.

In this paper, we have performed *in vitro* reconstitution experiments based on Giant Unilamellar Vesicles (GUVs) and confocal microscopy, where we have shown the absence of binding of AS to membranes containing GM1, even at relatively high GM1 content. We have next compared AS binding to membranes made of monounsaturated lipids or DPhPC (respectively), with increasing amounts of the corresponding negatively charged phosphatidylglycerol (PG). We have measured a much stronger affinity of AS for membranes made of DPhPC, and a reinforcement of this effect in the presence of PG lipids, as expected from former studies.[14,38] Our results are in very good agreement with our all-atom MD simulations that demonstrate that DPhPC, due to methyl-branches, promotes shallow lipid-packing defects within bilayers to a larger extent than polyunsaturated and monounsaturated lipids.

Materials and methods

AS purification and labeling

Recombinant wild type (WT) human AS was expressed and purified as described previously.[55] AS concentration was determined spectrophotometrically using an extinction coefficient of 5960 M^{-1} cm^{-1} at 280 nm. Pure AS (0.2–0.5 mM) in 50 mM Tris–HCl, pH 7.5, 150 mM KCl (buffer A) was filtered through sterile 0.22 μm filters and stored at −80 °C. Prior to labeling monomeric AS was purified by size exclusion chromatography using a Superose®6 HR10/30 column (GE Healthcare) equilibrated in phosphate buffered saline (PBS) buffer. Monomeric AS was labeled by addition of 2 molar excess of the aminoreactive fluorescent dye Alexa Fluor 488 (Alexa Fluor 488; Invitrogen, Carlsbad, CA). Labeling was performed for 30 minutes on ice following the manufacturer's recommendations. Unreacted dye was removed by size exclusion chromatography (NAP-10 column, GE-Healthcare, equilibrated in PBS). The amount of incorporated Alexa Fluor 488 was assessed by MALDI-TOF mass spectrometry, confirming that the average number of label per AS was 1.

GUV preparation

1,2-Dioleoyl-*sn-glycero*-3-phosphocholine (DOPC), 1,2-diphytanoyl-*sn-glycero*-3-phosphocholine (DPhPC), 1,2-dioleoyl-*sn-glycero*-3-phospho-(1′-*rac-glycerol*) (DOPG), 1,2-diphytanoyl-*sn-glycero*-3-phospho-(1′-*rac-glycerol*) (DPhPG), Ganglioside GM1 from ovine brain (GM1), cholesterol (ovine wool, >98%) (Chol) and egg phosphatidylcholine (EPC) were obtained as powder from Avanti polar lipids and dissolved into Chloroform (puriss p.a., Sigma Aldrich, ethanol stabilized). The lipid tracer BodipyTR Ceramide (Life technologies) was used at a concentration of 0.1 mol%. Cholera Toxin B-Subunit (CTxB) – Alexa 488 conjugate was obtained from Life technologies. Buffers were prepared with MilliQ water, 20 mM TRIS HCl pH 7.5 (Sigma), 100 mM KCl (Sigma). Buffers for the vesicle growth contained 200 mM sucrose (Sigma) and were osmotically matched to the observation buffer containing 200 mM glucose to facilitate GUV sedimentation. GUVs containing GM1 were prepared in a 20 mM Hepes pH 7.5 (Sigma) growth buffer containing 200 mM sucrose, osmotically matched to a 20 mM Hepes pH 7.5, 100 mM NaCl (Sigma) observation buffer. GUVs were formed by one of four established methods: spontaneous swelling,[42] gel assisted swelling on a polyvinyl alcohol (PVA) gel,[43] electroformed on platinum (Pt) wires,[44] or on indium tin oxide (ITO) slides.[41] For the spontaneous swelling of GUV containing 50% GM1, 100 μl of a solution of lipids at 0.5 mg ml^{-1} were deposited in a glass vial and dried using nitrogen gas then waiting 4 h in a vacuum oven. Lipids were then re-hydrated in growth buffer overnight. For gel assisted swelling PVA (MW 145 000, Merck KGaA) was dissolved at 5 mg ml^{-1} in 300 mM sucrose and applied on a plasma-cleaned cover slide. After the gel dried at 60 °C for 1 h, 10 μl lipids (3 mg ml^{-1}) were spread on the gel with a sterile metal rod. Lipids were desiccated for 30 min and subsequently rehydrated for 30 min in growth buffer. For the electroformation on Pt wires, 4 μl lipids (3 mg ml^{-1}) were spread on two 3 cm long wires (99.9%+, diameter 0.5 mm, Goodfellow, wire distance 3 mm) and desiccated for 30 min. The lipids were rehydrated in growth buffer for 12 h while a 500 Hz sinusoidal AC field (0.35 V root mean square (rms)) was applied to the wires. For the electroformation on ITO, 10 μl lipid solution at 0.5 mg ml^{-1} was spread and dried on the surface of two conductive slides (Präzisions Glas and Optik, GmbH). After assembling a chamber with the 2 slides and a space of 1 mm,

the lipid films were rehydrated in growth buffer. GUVs were swollen for 60 min under a sine voltage (1.1 V peak–peak, 10 Hz).

Imaging

10 μl of the GUV suspension from the growth chamber was transferred to a micro centrifugation tube and gently mixed with 89 μl observation buffer and 1 μl AS stock solution (100 μM) for a final AS concentration of 1 μM. Vesicles were incubated for 1 h before being transferred to a beta-casein (Sigma Aldrich) passivated observation chamber for imaging.

When indicated, images were acquired with a Nikon Eclipse TE2000-E equipped with Nikon PlanApoVC 60×, NA 1.40 objective, a CSU22 (Yokogawa) spinning disk unit and a Coolsnap HQ2 (Photometrics) camera. Samples were excited with 488 nm and 543 nm laser lines; emission was filtered with a GFP-mCherry filter set.

Images for the quantification were obtained with a Nikon Eclipse Ti microscope equipped with a confocal C1 unit and Nikon objective Plan Fluor 100× NA1.3. Alexa488 was excited with the 488 nm line of an Argon laser and BodipyTR was excited with a 543 nm He–Ne laser. Emission light collected in the green channel has a wavelength of 500–530 nm and the magenta channel of 568–642 nm. Images for the quantification were taken with the same imaging parameters for each condition in the center of the field of view.

Protein fluorescence was quantified by averaging the fluorescence along the equator of the vesicle thereby creating an intensity profile perpendicular to the membrane.[56] The profile was fit to the sum of a Sigmoid function, a Gaussian function and a first order polynomial. The rationale is that the Sigmoid accommodates the different AS concentration in- and outside the GUV, the Gaussian fits the membrane fluorescence and the polynomial accommodates offset and uneven imaging occurring out of the exact center of the picture. Membrane fluorescence (F_M) was obtained from the magnitude of the Gaussian. The bulk fluorescence (F_{bulk}) was measured as the average fluorescence intensity 20 pixels outside the vesicle. Since fluorescence is proportional to the amount of fluorophores in the focal volume and free dye was removed during protein labeling, the ratio F_M/F_{bulk} represents the amount of protein bound to the membrane inside the focal volume normalized to the amount of proteins in the focal volume in the bulk.

Molecular Dynamics Simulations

Three pure lipid bilayers, composed of 100% 1,2-dioleoyl-*sn-glycero*-3-phosphocholine (DOPC), 100% 1-stearoyl-2-arachidonoyl-*sn-glycero*-3-phosphocholine (SAPC) and 100%, 1,2-diphytanoyl-*sn-glycero*-3-phosphocholine (DPhPC) were considered in this study. Each lipid bilayer consisted of 288 lipids and it was fully solvated with 40 to 50 water molecules per lipid. Initial coordinates for DOPC and DPhPC were generated starting from smaller system downloaded from http://terpconnect.umd.edu/~jbklauda/research/download.html and http://simulo.apchem.nagoya-u.ac.jp/personal/wshinoda/index.html respectively, while initial coordinates for SAPC were generated using CHARMM-GUI.[57] Each system was initially minimized and shortly equilibrated for 200 ps, before a run of 200 ns. Only the last 100 ns were considered production run and thus analyzed.

The CHARMM36 force field[58] was used for all lipids. Parameters for SAPC were taken from ref. 59 and parameters for DPhPC were taken from ref. 53. The TIP3P model was used to describe water molecules.[60]

All simulations were performed using GROMACS 4[61] within the NPT ensemble. All systems were equilibrated with the Berendsen thermostat at 303 K (with a time constant of 0.1 ps; lipids and water coupled separately) and the Berendsen barostat at 1 bar (with a time constant of 1 ps and a compressibility of 4.5×10^{-5} bar^{-1}).[62] Production runs were run at 303 K using the velocity-rescaling thermostat[63] (with a time constant of 1 ps, lipids and water coupled separately) and at 1 bar using the Parrinello–Rahman barostat[64] (with a time constant of 5 ps and a compressibility of 4.5×10^{-5} bar^{-1}). Pressure coupling was applied semi-isotropically (x and y directions coupled, z direction scaled independently from x and y). Periodic boundaries were applied in all directions. Bond lengths were constrained using the P-LINCS algorithm.[65] A time step of 2 fs was used with the leap-frog integrator. Trajectories were initiated by assigning a Maxwell–Boltzmann distribution of velocities at the chosen temperature. Water molecules were kept rigid using the SETTLE algorithm.[66] Lennard-Jones interactions were cutoff at 1.2 nm. The smooth particle-mesh-Ewald (PME) method[67,68] was used for evaluating electrostatic interactions, with a real space cutoff of 1.0 nm, a grid of 0.15 nm^{-1} and an interpolation order of 6. The neighbor list was updated every 10 steps. Frames were saved every 10 ps for subsequent analysis.

Packing defects were defined and evaluated using a recently reported methodology.[26] In brief, the plane perpendicular to the membrane normal is mapped into a grid of 0.1 nm^2 resolution and the normal to the membrane plane is scanned for each grid point starting from the solvent and diving up to 0.1 nm below the sn-2 carbon of the glycerol. If no atom is met, we define the grid point as a "deep defect", if an aliphatic atom is met, we define the grid point as a "shallow defect". Adjacent elementary points of similar nature were then merged, resulting in defects of various sizes.

Defects were computed every 100 ps. The histograms of the computed packing defects *versus* defect size, normalized with respect to the total surface area analyzed, were then fitted with a single exponential distribution $y = A \times \exp(-x/x_0)$ for $x > 0.2$ nm^2. The resulting x_0 values are the packing defect size constants used throughout the text. Error bars shown in the text are standard errors in x_0 values estimated during the fitting procedure.

Results and discussion

1. Binding of AS to Giant Unilamellar Vesicles

To decouple AS affinity to curvature[24] from its affinity to a specific lipid, AS binding was quantified using Giant Unilamellar Vesicles (GUVs) with typical diameters of the order of tens of microns. The membrane of a GUV can be considered flat on a molecular

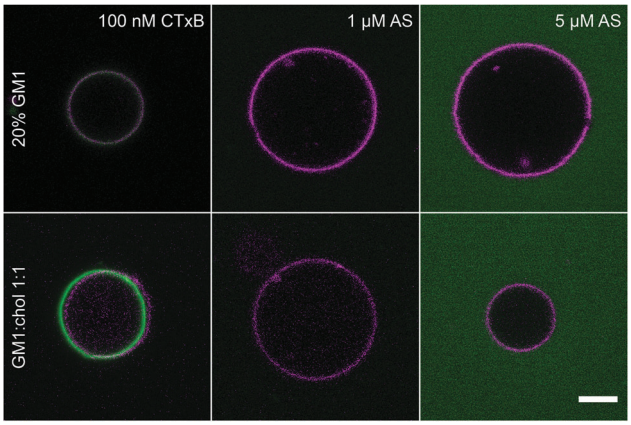

Fig. 1 AS binding to GM1-containing GUVs. GUVs containing 20% GM1 were prepared by electroformation (upper row), and GUVs of composition GM1 : chol 1 : 1 were prepared by spontaneous swelling (lower row). The GUV membrane is labeled with BodipyTR Ceramide (magenta). Two AS concentrations were tested (1 μM and 5 μM), as well as cholera toxin B-subunit (CTxB) as a control. The PMT gains in the protein channel (green) were (from left to right): 120, 110, 90 (upper row); 85, 110, 100 (lower row). Scale bar, 5 μm.

scale because the size of the GUV is much larger than the lipid bilayer thickness (typically 5 nm). We quantified AS binding to GUVs using confocal fluorescence microscopy, either with laser scanning or spinning disk microscopes.

GUVs containing gangliosides. We first checked if AS could bind GUV membranes made of 20% GM1, 15% cholesterol (Chol) and 65% egg phosphatidylcholine (EPC); this GM1 concentration is relevant for the density of this ganglioside in neuron membranes. Indeed, gangliosides represent 10% of neuron total lipid content[20] and GM1 represents 10 to 30% of them, depending on the brain cell type.[39] To this end, pure AS was labelled with Alexa 488 maleimide with a ratio of 1 Alexa fluorophore per AS on average. In agreement with a previous report,[40] we didn't detect any interaction of this label with GUVs. GUVs were prepared with the electroformation method on ITO slides[41] or, in the case of 50% GM1, with spontaneous swelling;[42] we confirmed the presence of GM1 in our GUVs by binding fluorescent cholera toxin (Fig. 1). However, at 1 μM or 5 μM, no binding of AS was detected on these GUVs, even when the GM1 density was increased to 50% using a spontaneous swelling method (Fig. 1). Our results differ from those published previously using either monolayers made up of pure gangliosides[18] or small liposomes containing 50% gangliosides mixed with lipids in a gel phase.[16] The discrepancy between our observations and those published previously suggests that

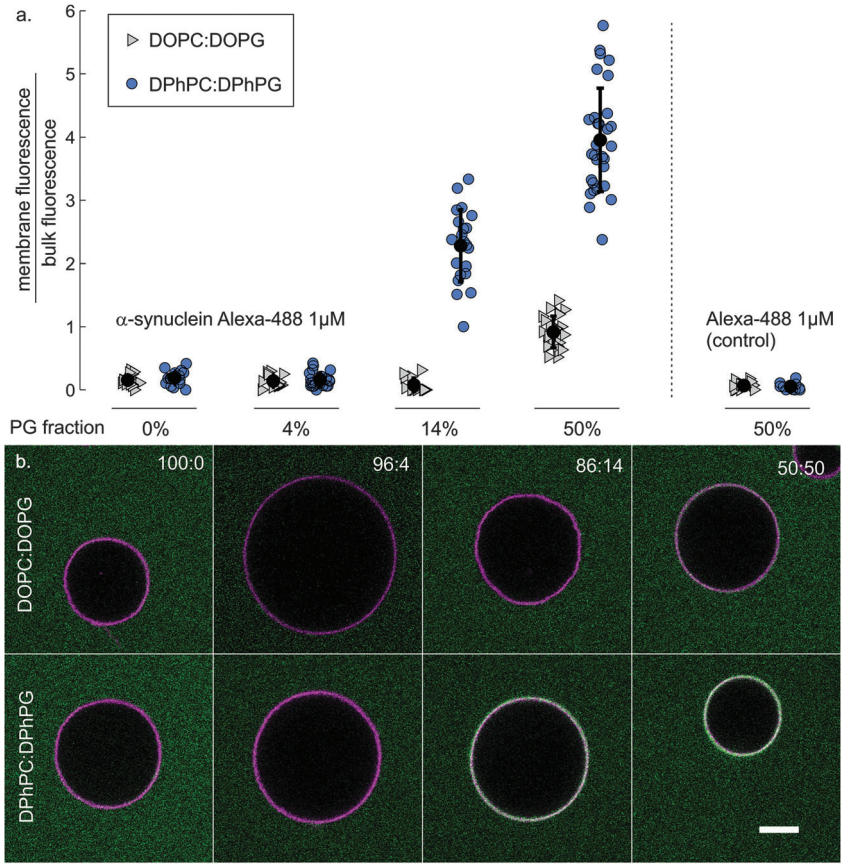

Fig. 2 AS binding to dioleoyl- and diphytanoyl-containing GUVs. (a) Relative quantity of AS bound to GUV membranes made of DPhPC or DOPC as a function of the fraction of PG lipids, assessed from the ratio of membrane to bulk AS fluorescence F_M/F_{bulk}. Black: mean ± standard deviation. (b) Representative images of GUVs chosen for the quantification of AS binding, containing increasing molar fractions of PG, as indicated on the images. Green: AS Alexa-488 1 μM, magenta: BodipyTR Ceramide. Bar: 5 μm.

specific or electrostatic interactions between AS and lipid head groups might not be sufficient for its binding to membranes, and that the lipid chains in the bilayer also contribute, in particular by producing lipid-packing defects as previously suggested.[22,23,25,27,29]

GUVs – branched chains *versus* unsaturated chains. To test the possible role of branched lipids on AS binding, we chose to compare dioleoyl (DO) lipids, that have a single unsaturation on each tail, with diphytanoyl (DPh) lipids that have two 4 fold methylated and fully saturated tails. Since AS binding to flat membranes is generally promoted by charged lipids[14,38] we supplemented phosphocholine (PC) lipids with phosphatidylglycerol (PG) starting at 50% mol/mol and decreasing stepwise to 0%. The results of the AS binding experiments to DO and DPh membranes are shown in Fig. 2a and representative images are shown in Fig. 2b. As expected for DO, AS binds to membranes containing 50% PG (binding was quantified from the ratio of membrane to bulk fluorescence, F_M/F_{bulk} = 0.9 ± 0.3 (mean ± s.d.)) but not to membranes containing only 14% PG. The DPh membrane, on the other hand, shows AS binding at 14% PG content (F_M/F_{bulk} = 2.3 ± 0.6). Remarkably, binding of AS to the DPh membrane containing 14% PG is stronger than to the DO membrane with 50% PG. When comparing both 50% PG compositions, binding to the DPh membrane (F_M/F_{bulk} = 4.0 ± 0.8) is 4.3× stronger than to the DO membrane. In contrast, control experiments with the free Alexa 488-maleimide did not show binding of the dye to GUVs with 50% PG (Fig. 2a).

The technique of PVA gel-assisted swelling of GUVs was chosen for these experiments[43] since it allows achieving a high yield at high content of charged lipids. Although the vesicles obtained through this method are reported to be free of detectable traces of gel in their membrane,[43] such contamination may still be present and alter binding. We therefore performed a control experiment with electroformed GUVs.[44] With this type of preparation, we found that AS binds to DPhPC GUVs without addition of PG (F_M/F_{bulk} = 0.8 ± 0.3). Pure DOPC GUVs nonetheless showed no binding, like in the case of GUVs with the PVA gel method. The difference of AS binding depending on the type of GUV preparation can have different origins. One possibility is that lyso-lipids and free fatty acids are formed during the electroformation as suggested in ref. 45. Another possibility is that the presence of PVA gel traces in the membrane may antagonize AS binding. However, both methods show qualitatively the same result: a much stronger AS affinity for DPh-containing membranes than for DO-containing membranes under equivalent conditions.

GUVs that do show AS binding are not fluctuating (floppy) but appear very spherical and tensed (Fig. 2), consistent with observations made at steady-state with different lipid compositions.[46] Additionally more than half of the GUVs (DO and DPh) show what appears to be a micron-size lipid–protein aggregate on the membrane, see Fig. 3, that is characterized by an increase in both lipid and protein fluorescence intensity and that is phenomenologically similar to those observed in a previous study of AS interacting with GUVs.[47] We observed that the aggregates are often accompanied by small vesicular buds (Fig. 3a) and exhibit a donut shaped structure (*i.e.* the aggregate is circular with a cavity in its center) (Fig. 3b–d). The organization of AS into nm-size ring structures was previously described from electron microscopy or AFM experiments;[48–51] however the organization of the lipid membrane and AS into a donut shape at a micrometer scale was never reported beforehand. Further investigation would require high-resolution light microscopy or electron microscopy to elucidate the structural details of GUV membrane reorganization.

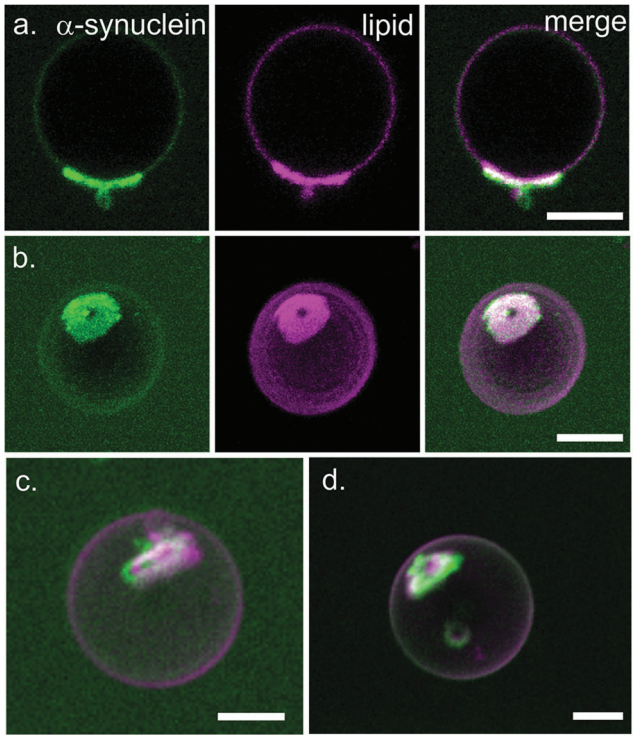

Fig. 3 Buds and donut-shaped lipid–protein aggregates on GUVs. Aggregates are present in more than half of the GUVs when AS is bound. A large fraction of these GUVs show structures that can be classified as buds or donuts. (a) Section of a donut-shape protein–lipid aggregate with a bud bulging out of the cavity. (b–d) Typical donut-shaped protein–lipid aggregates. Images are *z*-projections of the GUVs. (a, b) DPhPC, electroformed, confocal image. (c) DOPC : DOPG 50 : 50, PVA assisted swelling, (d) DPhPC : DPhPG 50 : 50, PVA assisted swelling. (a, b) Confocal images (c, d) spinning disk images. Green channel: AS-A488 1 μM. Magenta channel: BodipyTR Ceramide. Bar: 5 μm.

Membrane remodeling by AS was described to go along with pore formation or disruption in membranes.[12,52] Since the optical sucrose–glucose contrast was preserved, and no fluorescent AS was detected in the lumen of the GUVs, we can however exclude spontaneous formation of pores larger than the size of the sugars and of the AS monomer. Taken together our observations agree with a study of the binding dynamics of AS to GUVs that suggests membrane remodeling by membrane thinning but no poration.[46]

In conclusion, the binding assay demonstrates that AS has unique membrane remodeling properties and displays increased affinity to DPh lipids when compared to DO lipids, even on flat membranes, showing that the lipid tail domain has a measurable impact on AS binding and suggesting the existence of lipid packing defects in DPh-containing bilayers.

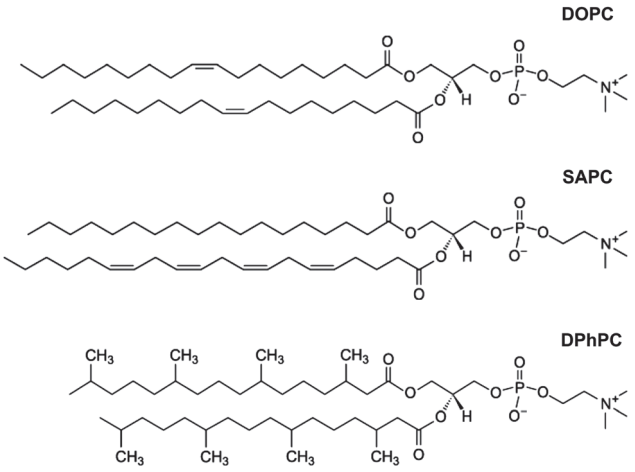

Fig. 4 Lipid chemical structures: 1,2-dioleoyl-*sn-glycero*-3-phosphocholine (DOPC), 1-stearoyl-2-arachidonoyl-*sn-glycero*-3-phosphocholine (SAPC) and, 1,2-diphytanoyl-*sn-glycero*-3-phosphocholine (DPhPC). DOPC is used as a reference lipid, while SAPC and DPhPC are used as model polyunsaturated and branched lipids, respectively.

2. Molecular surface properties of branched lipids

Next, we decided to investigate the origin of the observed binding of AS to branched lipids at the molecular scale. Recently, it was proposed that AHs, like those formed by AS, may be able to sense lipid-packing defects in lipid bilayers and that this property may be quantified *in silico*.[25,26,28] However, lipid-packing defects were shown to arise when unsaturated acyl chains were incorporated into the bilayer, while saturated lipids did not promote their formation and prevented binding of AHs to the bilayer surface.[27] Thus, our observation that saturated lipids, such as DPhPC, promote binding of AS to lipid bilayers may appear at first in contrast with these previous findings.

To investigate the effect of DPhPC on molecular properties of lipid bilayers, we decided to perform all-atom molecular dynamics (MD) simulations of lipid bilayers composed of three lipids displaying widely different chemistry: DOPC, consisting of two monounsaturated acyl chains, SAPC, consisting of a saturated acyl chain and a polyunsaturated acyl chain, and DPhPC, consisting of two saturated acyl chains each carrying four methyl groups (Fig. 4). In our analysis, we focused on the presence of lipid-packing defects for these three compositions, and in particular on "shallow" defects, *i.e.* exposed hydrophobic patches that do not extend deeply below the bilayer surface, since binding of AS has been shown to correlate to the presence of these defects in lipid bilayers.[29] A thorough and elegant description of DPhPC lipid bilayer properties can be found in ref. 53 and references therein.

Using a previously developed methodology, we thus computed both deep and shallow lipid-packing defects for the three lipid compositions (Fig. 5). In agreement with previous results obtained using coarse-grain MD simulations,[29] we observed that SAPC, a polyunsaturated lipid, does not promote the formation of deep packing defects, while substantially increasing the number and size of shallow defects in comparison with bilayers composed of mono-unsaturated acyl chains (DOPC). DPhPC, conversely, appears to increase both deep and shallow defects (Fig. 5). The increase is particularly marked for shallow defects, which are even more abundant in DPhPC than in polyunsaturated lipids such as SAPC.

On the one hand, these data rationalize the observed increased binding of AS to DPhPC-enriched lipid bilayers (Fig. 2), since lipid-packing defects promote the binding of peripheral proteins that use hydrophobic insertions to partition to the membrane environment. On the other hand, they suggest that acyl chain poly-unsaturation and the addition of methyl branches may be two distinct evolutionary strategies to promote adsorption of specific peripheral protein to the membrane surface.

Polyunsaturated lipids, in fact, promote the formation of shallow lipid packing defects[29] mostly thanks to their

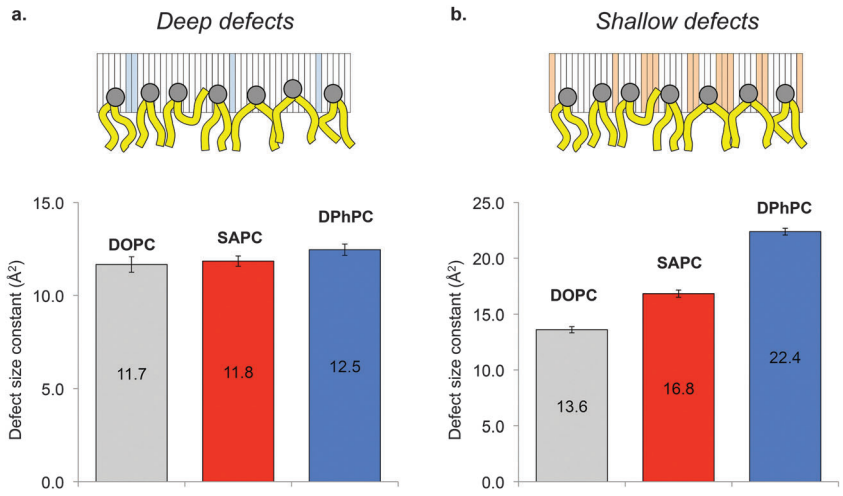

Fig. 5 Lipid-packing defects in all-atom molecular dynamics simulations. Deep (a) and shallow (b) lipid packing defects in all-atom molecular dynamics simulations of DOPC, SAPC and DPhPC lipid bilayers. The defect size constants shown are the fit to the single exponential distribution obtained by plotting the defect occurrence as a function of their size (see ref. 26 for a more thorough description of the method). The prefactors of the exponential fit are identical for the three lipid composition.

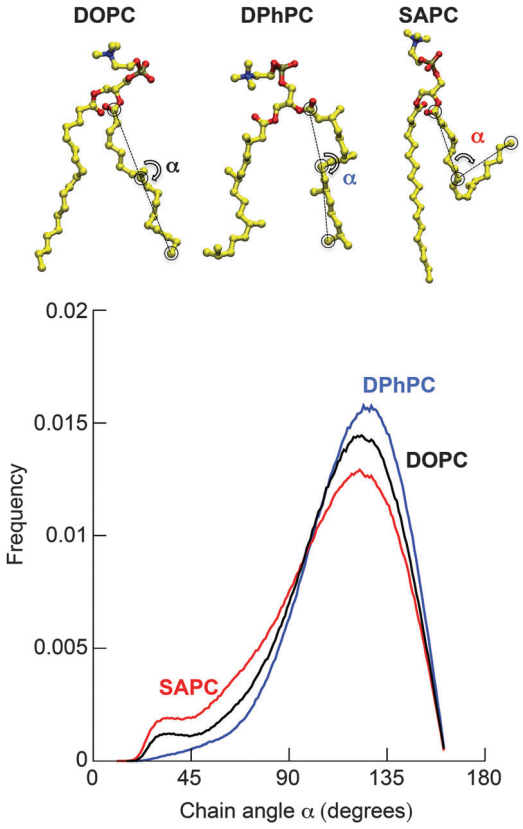

Fig. 6 Acyl chain conformational flexibility. Angular distribution between initial, middle and terminal carbon atoms of the sn2 mono-unsaturated acyl chains of DOPC (black), poly-unsaturated acyl chain of SAPC (red) and saturated branched chains of DPhPC (blue) in all-atom MD simulations. DPhPC acyl chains show a higher population in the extended conformation ($\alpha \approx 130°$), while mono- and poly-unsaturated acyl chains can adopt kinked ($\alpha \approx 35°$) conformations.

conformational flexibility, being able to backflip and emerge towards the aqueous environment, as exemplified by their angular distribution (Fig. 6). This phenomenon is completely absent in branched lipids, but is compensated by a dramatic increase in area per lipid (0.78 nm^2 for DPhPC at 303 K *vs.* 0.70 nm^2 for SAPC at 303 K in our MD simulations). Thus, shallow lipid packing defects in DPhPC ultimately result from the increase both in acyl chain disorder[54] and spacing between lipids.

Conclusion

The membrane binding properties of AHs play a crucial role in their physiological function, yet the interaction of AHs with lipid bilayers is not entirely understood. Here we have shown that methyl-branched acyl chains promote the adsorption of AS, an AH-containing protein that is abundant in brain tissues, to membranes by increasing the number and size of membrane lipid-packing defects. Since this mechanism is quite general,[27] we expect that methyl-branched lipids may favor the adsorption of different AHs to lipid bilayers, and especially AHs that have been shown to be able to sense membrane curvature.[27] Our results indicate that both hydrophobic and electrostatic interactions are crucial to modulate the binding of AS with complex lipid membranes.

Shallow lipid-packing defects, in particular, correlate well with the membrane adsorption properties of AS. These defects are promoted by both methyl-branched and polyunsaturated lipids,[29] but they originate from remarkably different molecular properties: enhanced chain flexibility for polyunsaturated lipids and increase in both acyl chain disorder and area per lipid for methyl-branched lipids.

Remarkably, these two lipid species have markedly contrasting mechanical properties: while polyunsaturated lipids significantly decrease membrane rigidity[69] and promote membrane deformations,[29] DPhPC is usually chosen as a model system in biophysical experiments because of its rigidity.[70,71] Thus, caution must be used in trying to correlate membrane elasticity and membrane binding properties of curvature-sensing AHs.[72,73]

Finally, DPhPC is generally used as a model lipid in electrophysiology studies.[33,34] Our data show that membrane adsorption of AHs is dramatically increased in the presence of this lipid; thus, special care must be taken when interpreting experiment involving methyl-branched lipids and AHs, and especially pore-forming toxins.

Acknowledgements

The authors thank G. Toombes and B. Antonny for highlighting discussions, and P. Fuchs for critically reading the manuscript. We thank M. Renner, A N. Shrivastava and A. Triller for promoting the interactions that triggered this project. We thank the BioImaging Cell and Tissue Core Facility of the Institut Curie (PICT-IBiSA) for technical support. This work was supported in part by funding from the Fondation Pierre Gilles de Gennes. M. G. was supported by an Institut Curie international PhD fellowship. P.B.'s group belongs to the French research consortium "CellTiss", to the Labex CelTisPhyBio (ANR-11-LABX0038) and to Paris Sciences et Lettres (ANR-10-IDEX-0001_02). R.M.'s group was supported by the Agence Nationale de la Recherche (ANR-11-BSV8-021-01) and a 'Coup d'Elan à la Recherche Française' award from Fondation Bettencourt Schueller.

References

1 J. Burré, M. Sharma, T. Tsetsenis, V. Buchman, M. R. Etherton and T. C. Südhof, *Science*, 2010, **329**, 1663–1667.
2 P. K. Auluck, G. Caraveo and S. Lindquist, *Annu. Rev. Cell Dev. Biol.*, 2010, **26**, 211–233.
3 L. Lourenço-Venda, S. J. Cragg, V. L. Buchman and R. Wade-Martins, *Trends Neurosci.*, 2010, **33**, 559–568.
4 H. J. Lee, C. Choi and S. J. Lee, *J. Biol. Chem.*, 2002, **277**, 671–678.
5 B. Antonny, *Annu. Rev. Biochem.*, 2011, **80**, 101–123.
6 C. C. Jao, B. G. Hegde, J. Chen, I. S. Haworth and R. Langen, *Proc. Natl. Acad. Sci. U. S. A.*, 2008, **105**, 19666–19671.
7 T. Bartels, J. G. Choi and D. J. Selkoe, *Nature*, 2011, **477**, 107–110.

8 C. M. Pfefferkorn, F. Heinrich, A. J. Sodt, A. S. Maltsev, R. W. Pastor and J. C. Lee, *Biophys. J.*, 2012, **102**, 613–621.

9 A. R. Braun, M. M. Lacy, V. C. Ducas, E. Rhoades and J. N. Sachs, *J. Am. Chem. Soc.*, 2014, **136**, 9962–9972.

10 J. Varkey, J. M. Isas, N. Mizuno, J. M. Borch, V. K. l. Bhatia, C. C. Jao, J. Petrlova, J. C. Voss, D. G. Stamou, A. C. Steven and R. Langen, *J. Biol. Chem.*, 2010, **285**, 32486–32493.

11 C. M. Pfefferkorn, Z. Jiang and J. C. Lee, *Biochim. Biophys. Acta, Biomembr.*, 2012, **1818**, 162–171.

12 N. P. Reynolds, A. Soragni, M. Rabe, D. Verdes, E. Liverani, S. Handschin, R. Riek and S. Seeger, *J. Am. Chem. Soc.*, 2011, **133**, 19366–19375.

13 K. Beyer, *Cell Biochem. Biophys.*, 2007, **47**, 285–299.

14 B. D. van Rooijen, M. M. Claessens and V. Subramaniam, *FEBS Lett.*, 2008, **582**, 3788–3792.

15 E. R. Middleton and E. Rhoades, *Biophys. J.*, 2010, **99**, 2279–2288.

16 Z. Martinez, M. Zhu, S. Han and A. L. Fink, *Biochemistry*, 2007, **46**, 1868–1877.

17 J.-Y. Park, K. S. Kim, S.-B. Lee, J.-S. Ryu, K. C. Chung, Y.-K. Choo, I. Jou, J. Kim and S. M. Park, *J. Neurochem.*, 2009, **110**, 400–411.

18 J. Fantini and N. Yahi, *J. Mol. Biol.*, 2011, **408**, 654–669.

19 H.-A. Hansson, J. Holmgren and L. Svennerholm, *Proc. Natl. Acad. Sci. U. S. A.*, 1977, **74**, 3782–3786.

20 E. Posse de Chaves and S. Sipione, *FEBS Lett.*, 2010, **584**, 1748–1759.

21 P. Brundin, R. Melki and R. Kopito, *Nat. Rev. Mol. Cell Biol.*, 2010, **11**, 301–307.

22 B. Nuscher, F. Kamp, T. Mehnert, S. Odoy, C. Haass, P. J. Kahle and K. Beyer, *J. Biol. Chem.*, 2004, **279**, 21966–21975.

23 M. M. Ouberai, J. Wang, M. J. Swann, C. Galvagnion, T. Guilliams, C. M. Dobson and M. E. Welland, *J. Biol. Chem.*, 2013, **288**, 20883–20895.

24 I. M. Pranke, V. Morello, J. Bigay, K. Gibson, J. M. Verbavatz, B. Antonny and C. L. Jackson, *J. Cell Biol.*, 2011, **194**, 89–103.

25 S. Vanni, L. Vamparys, R. Gautier, G. Drin, C. Etchebest, P. F. Fuchs and B. Antonny, *Biophys. J.*, 2013, **104**, 575–584.

26 L. Vamparys, R. Gautier, S. Vanni, W. F. Bennett, D. P. Tieleman, B. Antonny, C. Etchebest and P. F. Fuchs, *Biophys. J.*, 2013, **104**, 585–593.

27 S. Vanni, H. Hirose, H. Barelli, B. Antonny and R. Gautier, *Nat. Commun.*, 2014, **5**, 4916.

28 H. Cui, E. Lyman and G. A. Voth, *Biophys. J.*, 2011, **100**, 1271–1279.

29 M. Pinot, S. Vanni, S. Pagnotta, S. Lacas-Gervais, L.-A. Payet, T. Ferreira, R. Gautier, B. Goud, B. Antonny and H. Barelli, *Science*, 2014, **345**, 693–697.

30 H. Lindsey, N. O. Petersen and S. I. Chan, *Biochim. Biophys. Acta, Biomembr.*, 1979, **555**, 147–167.

31 N. P. Ulrih, D. Gmajner and P. Raspor, *Appl. Microbiol. Biotechnol.*, 2009, **84**, 249–260.

32 S. Wang and R. G. Larson, *Phys. Chem. Chem. Phys.*, 2014, **16**, 7251–7262.

33 A. O'Connell, R. Koeppe and O. Andersen, *Science*, 1990, **250**, 1256–1259.

34 M. Sondermann, M. George, N. Fertig and J. C. Behrends, *Biochim. Biophys. Acta, Biomembr.*, 2006, **1758**, 545–551.

35 M.-T. Lee, W.-C. Hung, F.-Y. Chen and H. W. Huang, *Biophys. J.*, 2005, **89**, 4006–4016.

36 J. D. Durrant, D. Caywood and D. D. Busath, *Biophys. J.*, 2006, **91**, 3230–3241.

37 E. Bárány-Wallje, S. Keller, S. Serowy, S. Geibel, P. Pohl, M. Bienert and M. Dathe, *Biophys. J.*, 2005, **89**, 2513–2521.

38 M. Stockl, P. Fischer, E. Wanker and A. Herrmann, *J. Mol. Biol.*, 2008, **375**, 1394–1404.

39 I. Kraĉun, H. Rösner, C. Ćosović and A. Stavljenić, *J. Neurochem.*, 1984, **43**, 979–989.

40 L. D. Hughes, R. J. Rawle and S. G. Boxer, *PLoS One*, 2014, **9**, e87649.

41 L. Mathivet, S. Cribier and P. F. Devaux, *Biophys. J.*, 1996, **70**, 1112–1121.

42 R. Kwok and E. Evans, *Biophys. J.*, 1981, **35**, 637–652.

43 A. Weinberger, F. C. Tsai, G. H. Koenderink, T. F. Schmidt, R. Itri, W. Meier, T. Schmatko, A. Schroder and C. Marques, *Biophys. J.*, 2013, **105**, 154–164.

44 P. Meleard, L. A. Bagatolli and T. Pott, *Methods Enzymol.*, 2009, **465**, 161–176.

45 N. F. Morales-Penningston, J. Wu, E. R. Farkas, S. L. Goh, T. M. Konyakhina, J. Y. Zheng, W. W. Webb and G. W. Feigenson, *Biochim. Biophys. Acta, Biomembr.*, 2010, **1798**, 1324–1332.

46 Z. Shi, J. N. Sachs, E. Rhoades and T. Baumgart, *Phys. Chem. Chem. Phys.*, 2015, DOI: 10.1039/C4CP05883F.

47 M. Grey, S. Linse, H. Nilsson, P. Brundin and E. Sparr, *J. Parkinson's Dis.*, 2011, **1**, 359–371.

48 H. A. Lashuel, B. M. Petre, J. Wall, M. Simon, R. J. Nowak, T. Walz and P. T. Lansbury Jr, *J. Mol. Biol.*, 2002, **322**, 1089–1102.

49 I. F. Tsigelny, P. Bar-On, Y. Sharikov, L. Crews, M. Hashimoto, M. A. Miller, S. H. Keller, O. Platoshyn, J. X. J. Yuan and E. Masliah, *FEBS J.*, 2007, **274**, 1862–1877.

50 T. T. Ding, S.-J. Lee, J.-C. Rochet and P. T. Lansbury, *Biochemistry*, 2002, **41**, 10209–10217.

51 K. A. Conway, S.-J. Lee, J.-C. Rochet, T. T. Ding, R. E. Williamson and P. T. Lansbury, *Proc. Natl. Acad. Sci. U. S. A.*, 2000, **97**, 571–576.

52 H.-Y. Kim, M.-K. Cho, A. Kumar, E. Maier, C. Siebenhaar, S. Becker, C. O. Fernandez, H. A. Lashuel, R. Benz, A. Lange and M. Zweckstetter, *J. Am. Chem. Soc.*, 2009, **131**, 17482–17489.

53 J. B. Lim and J. B. Klauda, *Biochim. Biophys. Acta, Biomembr.*, 2011, **1808**, 323–331.

54 W. Shinoda, M. Mikami, T. Baba and M. Hato, *J. Phys. Chem. B*, 2003, **107**, 14030–14035.

55 M. Ghee, R. Melki, N. Michot and J. Mallet, *FEBS J.*, 2005, **272**, 4023–4033.

56 M. Safouane, L. Berland, A. Callan-Jones, B. Sorre, W. Römer, L. Johannes, G. E. Toombes and P. Bassereau, *Traffic*, 2010, **11**, 1519–1529.

57 S. Jo, T. Kim, V. G. Iyer and W. Im, *J. Comput. Chem.*, 2008, **29**, 1859–1865.

58 J. B. Klauda, R. M. Venable, J. A. Freites, J. W. O'Connor, D. J. Tobias, C. Mondragon-Ramirez, I. Vorobyov, A. D. MacKerell, Jr. and R. W. Pastor, *J. Phys. Chem. B*, 2010, **114**, 7830–7843.
59 J. B. Klauda, V. Monje, T. Kim and W. Im, *J. Phys. Chem. B*, 2012, **116**, 9424–9431.
60 W. L. Jorgensen, J. Chandrasekhar, J. D. Madura, W. Impery and M. L. Klein, *J. Chem. Phys.*, 1983, **79**, 926–935.
61 D. Van Der Spoel, E. Lindahl, B. Hess, G. Groenhof, A. E. Mark and H. J. Berendsen, *J. Comput. Chem.*, 2005, **26**, 1701–1718.
62 H. J. C. Berendsen, J. P. M. Postma, W. F. van Gunsteren, A. DiNola and J. R. Haak, *J. Chem. Phys.*, 1984, **61**, 3684–3690.
63 G. Bussi, D. Donadio and M. Parrinello, *J. Chem. Phys.*, 2007, **126**, 014101.
64 M. Parrinello and A. Rahman, *J. Appl. Phys.*, 1981, **52**, 7182–7190.
65 B. Hess, H. Bekker, H. J. C. Berendsen and J. G. E. M. Fraaije, *J. Comput. Chem.*, 1997, **18**, 1463–1472.
66 S. Miyamoto and P. A. Kollman, *J. Comput. Chem.*, 2004, **13**, 952–962.
67 T. Darden, D. York and L. Pedersen, *J. Chem. Phys.*, 1993, **98**, 10089–10092.
68 U. Essmann, L. Perera, M. L. Berkowitz, T. Darden, H. Lee and L. G. Pedersen, *J. Chem. Phys.*, 1995, **103**, 8577–8593.
69 W. Rawicz, K. C. Olbrich, T. McIntosh, D. Needham and E. Evans, *Biophys. J.*, 2000, **79**, 328–339.
70 V. Vitkova, P. Meleard, T. Pott and I. Bivas, *Eur. Biophys. J.*, 2006, **35**, 281–286.
71 S. Tristram-Nagle, D. J. Kim, N. Akhunzada, N. Kufçerka, J. C. Mathai, J. Katsaras, M. Zeidel and J. F. Nagle, *Chem. Phys. Lipids*, 2010, **163**, 630–637.
72 F. Campelo and M. M. Kozlov, *PLoS Comput. Biol.*, 2014, **10**, e1003556.
73 A. J. Sodt and R. W. Pastor, *Biophys. J.*, 2014, **106**, 1958–1969.